Structures of Five Mutants of Toxic Shock Syndrome Toxin-1 with Reduced Biological Activity[†,‡]

Cathleen A. Earhart,[§] David T. Mitchell,[§] Debra L. Murray,[||] Denise M. Pinheiro,[⊥] Masazumi Matsumura,[⊥,#] Patrick M. Schlievert,[||] and Douglas H. Ohlendorf*[,§]

Department of Biochemistry, Medical School, University of Minnesota, Minneapolis, Minnesota 55455, Department of Microbiology, Medical School, University of Minnesota, Minneapolis, Minnesota 55455, and Nexstar Pharmaceuticals, Inc., Boulder, Colorado 80301

Received September 4, 1997; Revised Manuscript Received March 5, 1998

ABSTRACT: The three-dimensional structures of five mutants of toxic shock syndrome toxin-1 (TSST-1) have been determined. These mutations are in the long central α helix and are useful in mapping portions of TSST-1 involved in superantigenicity and lethality. The T128A, H135A, Q139K, and I140T mutations appear to reduce superantigenicity by altering the properties of the T-cell receptor interaction surface. The Q136A mutation is at a largely buried site and causes a dramatic change in the conformation of the $\beta7-\beta9$ loop which covers the back of the central α helix. As this mutation has the unique ability to reduce the toxin's lethality in rabbits while retaining its superantigenicity, it raises the possibility that this rear loop mediates the ability of TSST-1 to induce lethality and suggests a route for producing nonlethal toxins for therapeutic development.

Toxic shock syndrome toxin-1 (TSST-1) was the first toxin shown to be associated with staphylococcal toxic shock syndrome (TSS). Today, TSST-1 is considered to be the cause of all or nearly all menstrual TSS and at least 50% of all nonmenstrual cases (*1*). TSS is a severe multisystem condition characterized by high fever, rash, hypotension, and skin desquamation (peeling) upon recovery. A related condition, RED (recalcitrant, erythematous, desquamating) disorder, which affects AIDS patients, appears to be due to TSST-1 and other staphylococcal toxins (*2*). TSST-1 has been found in the kidneys of 18% of children who have died of sudden infant death syndrome (*3*). Finally, a recent study (*4*) has shown that organisms producing TSST-1 may be present in 60−70% of cases of Kawasaki syndrome, an illness typically seen in children younger than 4 years of age and which shares many features with TSS (*5*). The possible role of TSST-1 in Kawasaki syndrome remains controversial.

TSST-1 is a pyrogenic toxin superantigen (PTSAg) produced by *Staphylococcus aureus*. PTSAgs are small, nonglycosylated proteins with molecular weights ranging from 22 000 to 30 000 that are produced by *S. aureus*, group A streptococci, and certain non-group A streptococci (*6*, *7*). These toxins are synthesized with an amino-terminal signal peptide sequence that is removed during toxin secretion. PTSAgs are extremely resistant to proteases, are generally stable to temperatures of 60 °C or higher, and survive a range of pH from 2.5 to 11. In addition to TSST-1, members of this group include the streptococcal pyrogenic exotoxin serotypes (SPEA, SPEC, SPEF, and SPEZ), the streptococcal superantigen (SSA) from *Streptococcus pyogenes*, and the staphylococcal enterotoxin serotypes (SEA, SEB, SEC_n, SED, SEE, SEG, SEH, and SEI).

The three-dimensional structures of several PTSAgs, i.e., SEA, SEB, SEC2, SEC3, SPEC, and TSST-1, have been determined (*8*−*15*). All of the PTSAgs share a similar bilobal structure (see Figure 1) with one domain (B) composed of a five-strand mixed β barrel and a second domain (A) built around a long central α helix lying against a five-strand β sheet. Despite the many overall structural similarities, TSST-1 has several unique structural features, including the absence of an α helix at the bottom of the β barrel domain between strands $\beta3$ and $\beta4$, the lack of a disulfide loop at the top of the β barrel domain, and the extent to which the long central α helix is covered on the front and rear of the molecule. Structures of complexes of SEB and TSST-1 with class II major histocompatibility complex (MHC) molecules (*16*, *17*) and of SEC with T-cell receptor (TCR; *18*) have also been reported.

TSST-1 shares numerous biological properties with the other PTSAgs, including the abilities to stimulate the proliferation of $CD4^+$ T-cells that display particular Vβ elements in their TCR (superantigenicity), to induce fever (pyrogenicity), to cause capillary leakage, and to enhance endotoxin shock (*6*). The T-cell proliferation results in a

[†] This work has been partially supported by grants from the National Institutes of Health (GM54384 to D.H.O. and AI22159 to P.M.S.) and from the Minnesota Supercomputer Institute to D.H.O. D.T.M. was supported by an NIH training grant (2-T32-HD07381).

[‡] Coordinates for the T128A, H135A, Q136A, Q139K, and I140T mutants have been deposited in the Brookhaven Protein Data Bank under accession codes 1TS2, 1TS3, 1AW7, 1TS4, and 1TS5, respectively.

* Corresponding author.

[§] Department of Biochemistry, Medical School, University of Minnesota.

[||] Department of Microbiology, Medical School, University of Minnesota.

[⊥] Nexstar Pharmaceuticals, Inc.

[#] Current address: Corixa Corp., Seattle, WA 98104.

S0006-2960(97)02189-2 CCC: $15.00
Published on Web 04/28/1998

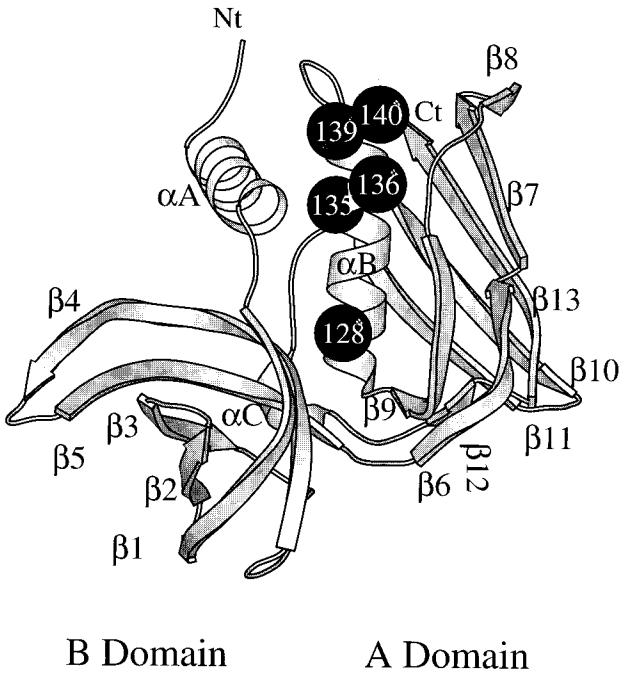

FIGURE 1: MOLSCRIPT (*51*) drawing of TSST-1. β strands are indicated with numbers; α helices are indicated with letters. Sites of mutants that were studied are indicated with black spheres.

massive release of cytokines, including those from T-cells and macrophages (*19*−*21*) that contribute significantly to capillary leakage. The ability of TSST-1 and the other PTSAgs to induce fever probably occurs as a result of the release of interleukin-1 and tumor necrosis factor-α (TNF-α) from macrophages as well as through direct effects on the hypothalamus (*22*, *23*). Also, TSST-1 has been shown to bind specifically to human and porcine endothelial cells. This direct interaction may contribute to the capillary leakage seen in TSS (*24*). The ability of TSST-1 and the other PTSAgs to enhance the lethal effects of endotoxin shock may result from their ability to block clearance of endotoxin by the liver (*25*−*27*). This effect does not depend on superantigenicity but may contribute to capillary leakage associated with cytokine release.

The properties of lethality and superantigenicity are separable as demonstrated by the Q136A mutation of TSST-1 which has reduced lethality in rabbits while maintaining superantigenicity (*28*). The K132E mutant of TSST-ovine (T19A/A55T/T57S/T69I/Y80W/I140T TSST-1) remains lethal but exhibits reduced mitogenicity (*14*, *29*). Several point mutations have resulted in decreased superantigenicity and lethality, including H135A, Q139K, and the T69I/Y80W/E132K/I140T tetramutant (huvine) (*29*−*32*). Crystallographic analyses of mutant TSST-1's have been undertaken to gain a better understanding of the structural foundations for the biological properties of TSST-1. We have recently reported the refined structures of wild type TSST-1 in three crystal forms and of the huvine tetramutant (*33*). Here we report the refined structures of the T128A, H135A, Q136A, I140T (*28*), and Q139K (*32*) mutants. All of these mutations are in the long central helix located between the A and B domains of TSST-1 and define the role of the α helix in lethality and mitogenicity.

MATERIALS AND METHODS

The T128A, H135A, Q136A, and I140T mutants were purified by ethanol precipitation from stationary phase cultures of *S. aureus* followed by isoelectric focusing gels as described by Blomster-Hautamaa and Schlievert (*34*); the Q139K mutant was expressed in *Escherichia coli* and purified by HPLC as described by Hurley et al. (*32*). All mutants were crystallized by vapor diffusion (*35*, *36*). Two microliters of a 10 mg/mL protein solution in distilled water was mixed with an equal volume of reservoir solution on a siliconized cover slip that was inverted over the reservoir and sealed with vacuum grease. The T128A, H135A, and I140T mutants were crystallized at pH 3.6−6.8 in 50 mM acetate buffer, 4−16% PEG 4000, and 1 M LiCl at 18 °C (*37*). The Q139K mutation was crystallized under the same conditions with the addition of 100−200 mM $MgCl_2$. Crystals of Q136A were obtained using a reservoir solution of 8−22% PEG 4000, 5−15% 2-propanol, and 100 mM HEPES (pH 7.5). Diffraction data were collected by a Siemens area detector using monochromated CuKα radiation generated by a Rigaku RU-200 rotating anode. The data frames were processed using the Xengen suite of programs (*38*). Data collection statistics are given in Table 1.

The structures of the Q136A, Q139K, and I140T mutants were solved by molecular replacement using XPLOR (*39*) with the refined structure of TSST-1 from the $C222_1$ crystal form (*33*). In the Q136A mutant, the model obtained after Patterson correlation refinement was refined by simulated annealing followed by rounds of visual inspection using TOM/FRODO (*40*), O (*41*), and INSIGHT (Biosym Corp., La Jolla, CA) and Powell minimization. Noncrystallographic symmetry restraints were not employed during the refinement to allow us to find differences between molecules in the asymmetric unit. However, during rebuilding, models were compared with that of the highly refined $C222_1$ crystal form as well as with other molecules in the asymmetric unit so they agreed with the noncrystallographic symmetry when warranted. The Q139K and I140T mutants were similarly solved and refined, but because of the reduced order of these mutants, normal independent thermal factor refinement was not performed. Experiments using a single thermal factor for each residue showed nonphysical differences between adjacent residues. Thus, we returned to individual thermal factor refinement with the thermal factor constraints tightened by decreasing the target σ's by a factor of 5 while increasing R_{WEIGHT} by the same factor. This protocol resulted in a rms difference of the thermal factors of bonded atoms of 0.25 Å^2 for the I140T mutant and of 0.40 Å^2 for the Q139K mutant. These values should be compared to 3.3 Å^2 for the Q136A mutant. In the I140T mutant, molecular replacement revealed that the two molecules in the asymmetric unit are related by a local 2-fold symmetry axis perpendicular to the crystallographic 6_1 axis generating a pseudo $P6_122$ cell. A similar pseudocell is found in the $C222_1$ crystal form of TSST-1 (*14*, *15*).

Since the T128A and H135A mutants were isomorphous with respect to the $C222_1$ crystal form of wild type TSST-1, the models were refined using Powell minimization after adjusting for the small changes in unit cell dimensions.

Table 1: Data Collection and Refinement Statistics

	T128A	H135A	Q136A	Q139K	I140T
diffraction data					
space group	$C222_1$	$C222_1$	$P1$	$R32$	$P6_1$
unit cell parameters	$a = 108.8$ Å $b = 177.4$ Å $c = 97.2$ Å	$a = 108.4$ Å $b = 176.6$ Å $c = 97.1$ Å	$a = 49.6$ Å $b = 99.3$ Å $c = 41.3$ Å $\alpha = 88.5°$ $\beta = 93.3°$ $\gamma = 91.1°$	$a = b = 152.4$ Å $c = 142.3$ Å	$a = b = 104.9$ Å $c = 98.2$ Å
no. of molecules/ asymmetric unit	3	3	4	2	2
observed reflections	441 613	672 210	157 168	64 169	115 253
unique reflections	38 992	63 452	50 028	8172	11 213
completeness (%)	91	100	79	99	99
resolution (Å)	20−2.3	20−2.0	20−1.95	20−3.4	20−3.1
R_{sym}	0.096	0.065	0.056	0.149	0.132
refinement data					
reflections ($F > 0$)	37 126	51 454	46 153	7865	10 845
R-factor	0.160	0.178	0.176	0.210	0.179
$\langle B \rangle$ for each molecule (Å^2)	23.7, 20.7, 23.9	23.4, 20.2, 23.9	24.7, 23.7, 25.8, 26.6	44.1, 67.3	15.7, 17.5
rms bond length (Å)	0.009	0.016	0.022	0.008	0.006
rms bond angle	1.74	2.60	2.37	1.76	1.59
no. of protein atoms	4671	4692	6248	3118	3116
no. of solvent molecules	188	241	291	0	20

RESULTS AND DISCUSSION

Table 1 provides the statistics regarding the final refined models of the five mutants. All non-zero reflections and a bulk solvent model were included in each refinement. The ribbon drawing presented in Figure 1 shows the positions of the TSST-1 mutants and the elements of secondary structure found in the refined structures of three crystal forms of native TSST-1, of the huvine tetramutant (*33*), and of TSST-1 in a complex with class II MHC (*17*). Among these crystals, the toxins show remarkably few variations. The most variable regions are the amino-terminal residues, the end of the $\beta4-\beta5$ loop, and the $\beta7-\beta9$ loop which covers the back of helix αB in the A domain (*33*, *42*). This observation is mirrored in these regions having some of the largest thermal factors in the molecule.

The differences between the Cα's of individual monomers of mutant toxins and monomer A of the wild type $C222_1$ crystal form are plotted in Figure 2. Plots of the differences of monomers A and C of the T128A and H135A mutants are not presented because the differences are smaller than those exhibited by monomer B. The mean rms difference for all Cα's ranges from 0.21 Å for the I140T mutant to 0.98 Å for the Q136A mutant. As was found for wild type TSST-1, the regions of highest variability are at the amino termini, the $\beta4-\beta5$ loop, and the $\beta7-\beta9$ loop.

T128A. Thr 128 is the fourth of the 17 residues in helix αB. In the $C222_1$ crystal form, the side chain is in the gauche$^+$ conformation with Thr 128 Cγ2 protruding into the solvent-exposed groove on the back of the molecule. Thr 128 Oγ1 forms two hydrogen bonds with solvent molecules and a hydrogen bond with the carbonyl O of Asn 65. The T128A mutant crystallizes isomorphously with the wild type $C222_1$ form. The 0.17−0.19 Å rms difference between the Cα's of the three molecules of T128A is comparable to the 0.16−0.21 Å observed between the molecules in the wild type $C222_1$ form. The rms difference between equivalent monomers of T128A and of the wild type $C222_1$ crystal form are 0.11, 0.08, and 0.12 Å for Cα′ and 0.48, 0.25, and 0.32 Å for all atoms. rms differences of this magnitude are within the range expected for the independent refinement of the same structure (*43*−*45*) and show that, for each individual molecule, changing Thr 128 to alanine makes no significant change in the structure. Globally, there is a shift of about 0.5 Å for the three monomers in the T128A mutant in addition to an increase in the thermal parameters of the solvent.

H135A. His 135 is found in the penultimate turn of helix αB in the A domain. It is between Gln 139 and Phe 131. In the wild type toxin, the side chain is 25% solvent-exposed with a hydrogen bond between His 135 Nδ1 and Tyr 13 O.

The most significant changes found in the H135A mutant are in the side chain conformation of Phe 131 and in the Ser 15−Gly 16 dipeptide. The electron density for the $C222_1$ form of wild type TSST-1 and for the huvine tetramutant indicates both trans and gauche$^-$ conformations are present for Phe 131 (*33*). In the H135A mutant, the electron density indicates only the gauche$^-$ conformation is present. This is apparently due to the abolition of favorable ring stacking interactions between the side chains of His 135 and Phe 131 in the trans conformation. Examination of $F_o - F_c$ maps for the H135A mutant revealed $\pm5-7\sigma$ features focused around the Ser 15−Gly 16 peptide bond. Flipping the peptide bond still results in $F_o - F_c$ map $\pm4-6\sigma$ features around this bond. Moreover, flipping this bond produces a short contact between the carbonyl oxygens of Ser 15 from symmetry-related molecules ($d < 2.5$ Å). In the wild type conformation, the closest contact for this region is 3.4 Å, between the amide nitrogens of Gly 16 from symmetry-related molecules. This flipped conformation was reported by Papageorgiou et al. (*46*) in their 2.5 Å resolution model of the H135A mutant. Our higher-resolution maps suggest that both peptide geometries are equally occupied. This allows the formation of a hydrogen bond between Gly 16 N and Ser 15′ O ($d = 2.7$ Å; see Figure 3). Both conformations must have equal occupancies because the contact between one of the pairs of molecules is crystallographic.

The 0.15−0.17 Å rms difference between the Cα's of the three molecules of H135A is comparable to the value of 0.16−0.21 Å observed between the molecules in the wild

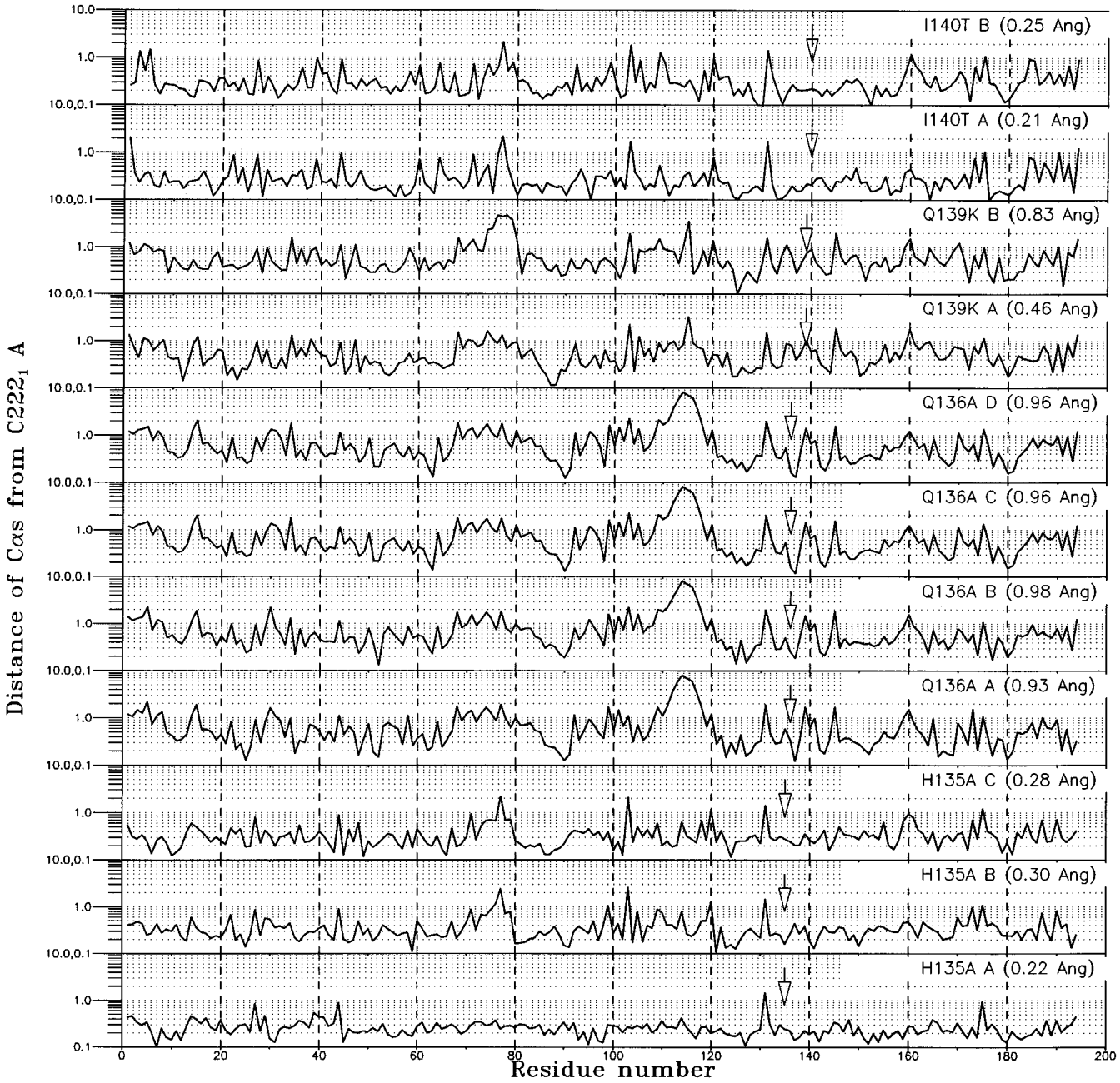

FIGURE 2: Coordinate differences of Cα's of mutants from those of molecule A of crystal form $C222_1$. The overall rms differences for the entire molecules are indicated. Arrows indicate mutated residues.

type $C222_1$ form. The rms differences between corresponding molecules in the H135A and wild type TSST-1 are 0.11−0.12 Å for the Cα's and 0.29−0.39 Å for all atoms, consistent with no significant overall structural change (*43*−*45*).

Q136A. The Q136A mutation crystallizes in space group *P*1 and diffracts to 1.95 Å resolution. The four molecules in the unit cell are very similar to each other with rms differences between molecules of 0.15−0.26 Å for Cα's and 0.56−0.68 Å for all atoms. In all four molecules, the $F_o - F_c$ and $2F_o - F_c$ maps indicated two side chain conformations for Phe 131 as found in the $C222_1$ crystal form of wild type TSST-1 and in the huvine tetramutant (*33*). The Ser 15−Gly 16 peptide is flipped relative to wild type TSST-1. There is substantial flexibility in the $\beta1-\beta2$ turn where a type II turn is found in all other TSST-1 structures. For molecule B, the density was strong enough to support flipping the carbonyl of Ser 30 to form a type I turn. In all four molecules, the $F_o - F_c$ maps indicate a variable population of both type I and type II turns at this location.

In the wild type TSST-1, Gln 136 is a nearly completely buried side chain on the penultimate turn of helix αB. Gln 136 Oϵ1 forms hydrogen bonds with His 141 Nϵ2 and Leu 113 N; Gln 136 Nϵ2 forms hydrogen bonds with Lys 114 O and a solvent molecule. In the Q136A mutant, Ala 136 cannot form these bonds and so the $\beta7-\beta9$ loop reorganizes with large shifts in Lys 114, Tyr 115, and Trp 116 in all four molecules (see Figure 4). In its new position, the aromatic side chain of Tyr 115 is positioned about 2.8 Å away from and roughly parallel to the position where the carbonyl of Gln 136 would have been. Thus, the new conformation of the $\beta7-\beta9$ loop would not be possible in wild type TSST-1. To confirm the new loop conformation, an omit map was calculated in which the occupancies of the

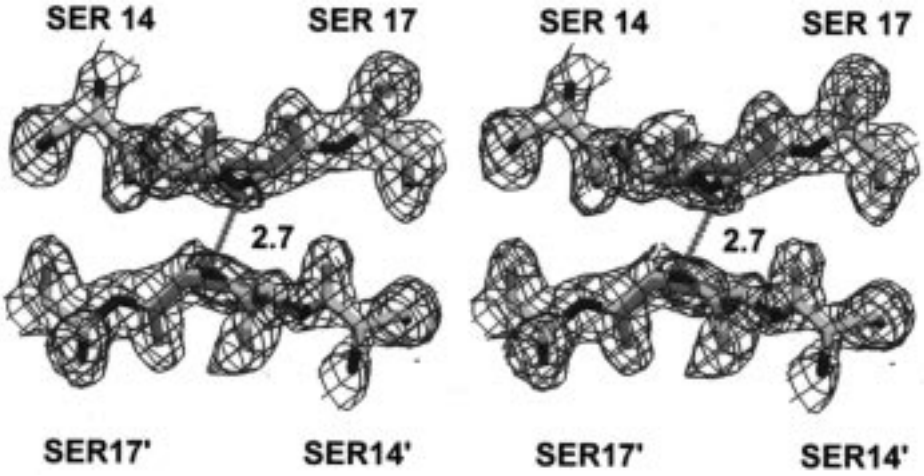

FIGURE 3: $2F_o - F_c$ density map for the H135A mutant around the crystallographic 2-fold symmetry axis near molecule B. Carbon atoms are yellow, nitrogen atoms blue, and oxygen atoms red. The alternate flipped conformation of the Ser 15−Gly 16 dipeptides is shown in green. The 2.7 Å distance between Gly 16 N and Ser 15′ O is indicated. This figure was created using SETOR (*52*).

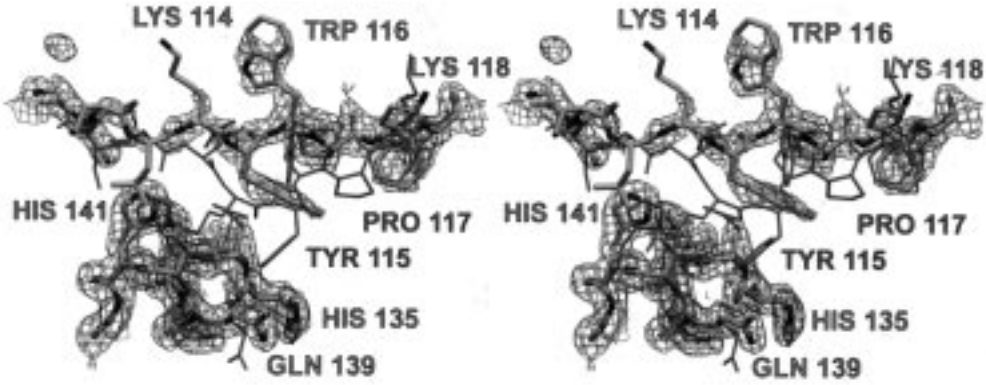

FIGURE 4: $2F_o - F_c$ density map for the Q136A mutant around residues 111−119 and 135−142. The conformation of this region in Q136A is shown with carbon atoms in yellow, nitrogen atoms in blue, and oxygen atoms in red with selected residues labeled in yellow. The conformation of this region in wild type TSST-1 is shown in green with selected residues labeled. This figure was created using SETOR (*52*).

residues in the loop were set to zero and a cycle of refinement was calculated. Although the density was somewhat fragmented, it clearly indicated the altered loop conformation existed.

The observation of a change in the $\beta7-\beta9$ loop in the Q136A mutant, the repositioning of Tyr 115 in the Q139K mutant, and the presence in this loop of some of the highest main chain thermal parameters in all known TSST-1 structures (*33*) leads one to consider the question of what factors influence the conformation of this region in general. In all three crystal forms of wild type TSST-1 and in the T128A, H135A, and I140T mutants, the dimers formed using the top surface of toxins are virtually identical. In Q136A and Q139K, however, the dimer is different (see Figure 5). This difference can be viewed as a rotation of approximately 15° around helix αA which opens the intermolecular interface, allowing the enhanced variability of the amino termini seen in Q136A and Q139K. This opening alleviates the close contact that can inhibit flipping of the carbonyl of Ser 15. The 1 Å shift seen for Ser 15 and Gly 16 in the Q136A mutant is partially due to this flip. It is clear that the details of the dimeric interaction are a consequence of the conformation of the $\beta7-\beta9$ loop and not vice versa because the wild type conformation is found in the huvine tetramutant (*33*) and in the TSST-1−MHC complex (*17*) where no dimer is formed.

Q139K. The Q139K mutant crystallizes in space group *R*32 with the lowest resolution (3.4 Å) of the five mutants presented. Gln 139 is the penultimate residue in helix αB, and its side chain carbonyl stacks on the side chain imidazole of His 135. In the wild type protein, Gln 139 Oϵ1 forms two potential hydrogen bonds with Thr 138 Oγ1 (2.8 Å) and Arg 145 NH2 (3.11 Å), while Gln 139 Nϵ2 forms a hydrogen bond with a solvent molecule. As Gln 139 is exposed to solvent, its mutation to lysine can be readily accommodated. Apparently, the change in space group is a consequence of the creation of a strongly basic patch by Arg 145, Lys 139, and His 135. In molecule A of the Q139K mutant, Lys 139 forms a charge pair with Glu 132 from a neighboring molecule.

The mean thermal factors for the two Q139K molecules in the crystallographic asymmetric unit are significantly higher than those found in other TSST-1 structures, with molecule B having the higher mean thermal factors of the two. To determine if there might have been an error during refinement, the Q139K structure was re-refined starting with simulated annealing using the *R*-free protocol (*47*; 10% of the data set aside). The *R*-factor and *R*-free dropped to 0.225 and 0.286, respectively, having started from 0.34, an indication of the veracity of the structural models. The high thermal factors of molecule B appear to arise from a relative lack of intermolecular contacts with its neighbors. The rms

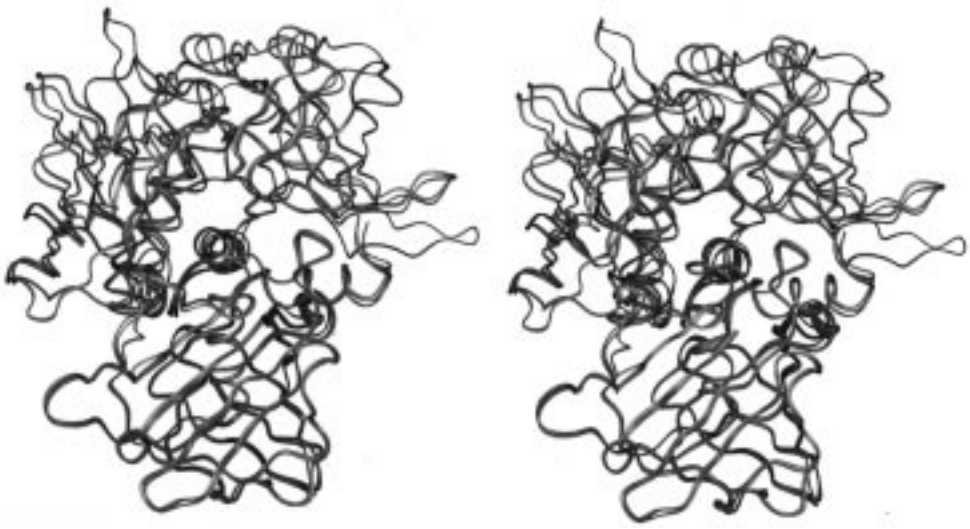

FIGURE 5: Ribbon drawings (in stereo) of wild type TSST-1 (blue), mutant Q139K (green), and mutant Q136A (orange) dimers. This figure was created using INSIGHT (Biosym Corp.).

differences between molecule A and the $C222_1$ form of wild type TSST-1 are <0.5 Å for Cα's and <1 Å for all atoms. These values are typical for proteins crystallized in different space groups (*43*, *45*). For molecule B, the corresponding rms differences are 0.8 and 1.1 Å, respectively. These larger differences are largely due to a 5 Å shift of the end of the $\beta4-\beta5$ duplex of molecule B required by contacts with adjacent molecules. This shift, present only in molecule B, can be broken down into two components, i.e., a 3.6 Å shift in the plane of the turn and a 2.8 Å perpendicular shift. The lateral shift is similar to that found in the TSST-1−MHC complex (*17*, *42*). Beyond the $\beta4-\beta5$ duplex, the largest shift is found at Tyr 115, 10 Å from Lys 139. In both molecules, the Cα of Tyr 115 has moved nearly 2 Å toward the carboxyl end of helix αB. This reduces the Cα−Cα distance between residues 115 and 139 from 9.9 to 8.4 Å. Although this change is present in both molecules in the Q139K mutant, we are uncertain that the mutation is the direct cause. Rather, the interactions with symmetry-related molecules preclude a wild type position for Tyr 115, suggesting that the observed change is a consequence of crystal packing.

I140T. Ile 140 is the final residue in helix αB. Although there are some small differences at the amino terminus, the end of the $\beta4-\beta5$ duplex and the $\beta10-\beta11$ turn, changing this exposed residue has no significant effect on the structure of TSST-1. The new Thr 140 Oγ1 is in the same place as Ile 140 Cγ1 in the wild type toxin, producing a potential long hydrogen bond with Lys 114 O (d = 3.5 Å) or Gln 136 Oϵ1 (d = 3.6 Å). The electron density maps do not support the rotated side chain conformation seen in the huvine tetramutant (*33*) where the Thr 140 Oγ1 forms two potential hydrogen bonds with Gln 136 O and Gln 136 Oϵ1. Overall, the rms difference from the $C222_1$ form of the wild type TSST-1 is 0.18−0.25 Å for Cα's and 0.62−0.70 Å for all atoms.

The I140T mutant of TSST-1 crystallizes in space group $P6_1$ under the same conditions as wild type TSST-1 and the H135A mutant crystallize in space group $C222_1$. As the latter two proteins crystallize with a noncrystallographic 3-fold coincident with the crystallographic screw axis, a pseudo-$P6_122$ cell is created with the following values: $a = b$ = 104.7 Å and c = 97.6 Å (*14*). In forming the $P6_1$ cell, the individual molecules rotate by less than 5° and move by less than 1 Å, making the alternating crystallographic and noncrystallographic dyads all noncrystallographic. The reason for this change is unknown. A relaxation of the dyad symmetry would allow additional variability in the Ser 15−Gly 16 peptide bond. Because of the reduced resolution observed in the I140T mutant, this speculation cannot be confirmed.

BIOLOGICAL ACTIVITIES

The mutants whose structures have been examined using X-ray crystallography fall into two categories: those that modulate lethality and superantigenicity jointly and those that modulate lethality and superantigenicity independently. Mutants which fall into the first class are the more common and include T128A, H135A, Q139K, and I140T.

The mutants with the largest joint reduction in superantigenicity and lethality are H135A and Q139K. As shown in Table 2, the H135A mutant has no significant superantigenicity with rabbit cells. This agrees with our previous observations (*28*) and with those of others using rabbit and human cells (*32*, *48*). In addition, this mutant has extremely low lethality in rabbits (*28*) as well as in a murine model (*48*). Hurley et al. (*32*) found that the Q139K mutant was unable to stimulate the production of IL-2 in a murine T-cell hybridoma and did not induce the proliferation of human peripheral blood leukocytes. As shown in Table 2, this mutant also has markedly reduced lethality in rabbits even at doses 2.5 times greater than the usual test dose.

The T128A and I140T mutants have only marginal effects on superantigenicity and lethality. Hurley et al. (*32*) found that the I140T mutant showed a reduced ability to stimulate murine cells to produce IL-2, although its binding of human class II MHC or the response of human peripheral blood leukocytes was not reduced. Deresiewicz et al. (*49*) also reported that the I140T mutant is indistinguishable from wild type TSST-1 in the latter assay with human cells. As determined here and by Murray et al. (*28*), the activity of the I140T mutant is reduced 10−24% compared to that of

Table 2: Superantigenicity and Lethality of Mutants Compared to Those of the Wild Type

wild type or mutant protein	IL-2 response[a]	proliferation of rabbit splenocytes (10^3) at different protein concentrations				lethality in the minipump assay (200 μg)
		1000 ng	100 ng	10 ng	1 ng	
native	+	299 ± 16	236 ± 12	221 ± 9.3	179 ± 11	3/3
T128A	ND[b]	204 ± 7.1	197 ± 9.8	194 ± 7.0	173 ± 4.2	3/3
H135A	−	0.0 ± 1.0	0.0 ± 0.6	4.1 ± 1.6	3.5 ± 3.4	0/3
Q136A	ND	56.4 ± 13	108 ± 15	130 ± 13	58.7 ± 16	0/3 (2 mg)
Q139K	−	ND	ND	ND	ND	0/3, 1/3 (500 μg)
I140T	−	227 ± 14	195 ± 12	200 ± 8.6	158 ± 11	3/3

[a] Ability of a mutant to stimulate a murine Vβ-expressing T-cell hybridoma to produce IL-2 as reported by Hurley et al. (*32*). [b] ND means not determined.

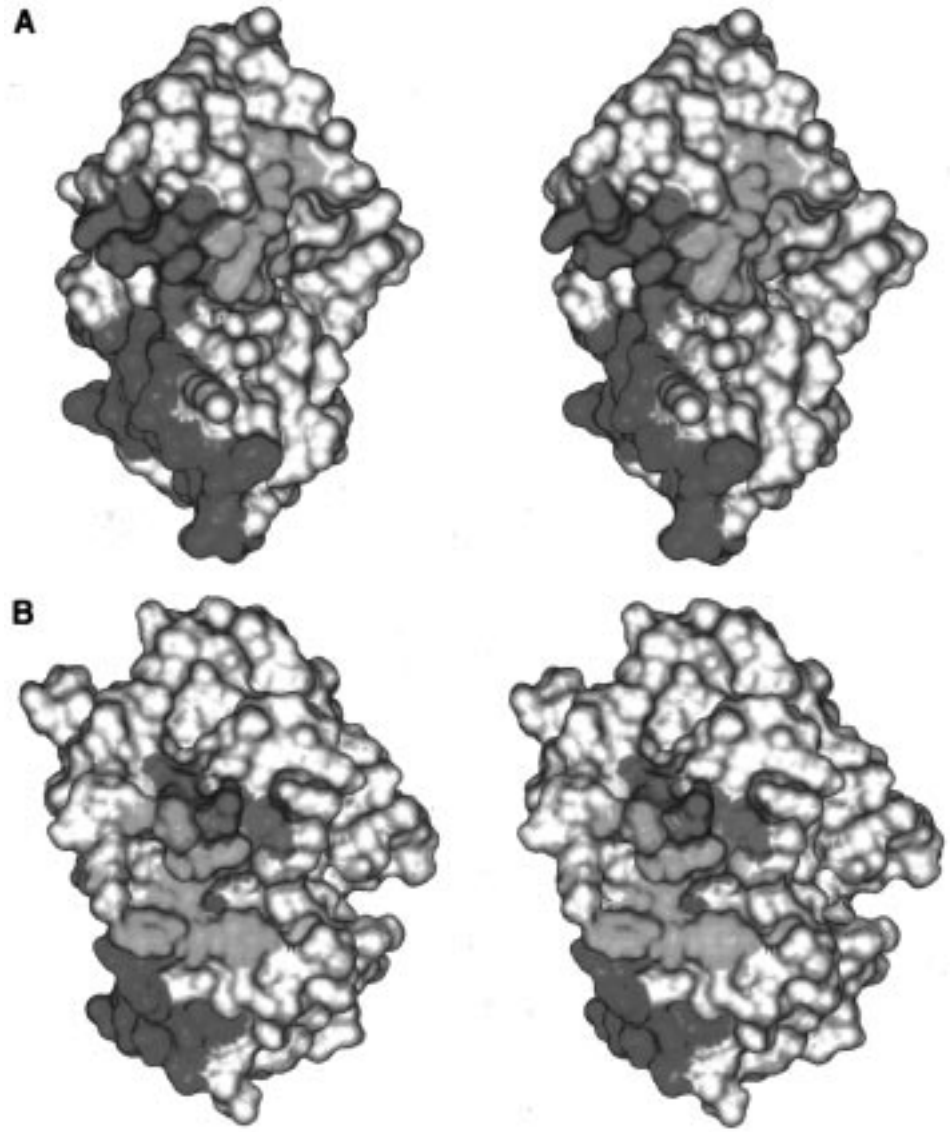

FIGURE 6: Top view (in stereo) of the solvent accessible surface of TSST-1 (A) and SEB (B). Residues in the class II MHC interface are shown in green; residues in the presumed TCR interface for SEB or which reduce superantigenicity and are outside the class II MHC interface for TSST-1 are shown in yellow. The amino-terminal helices of SEB and TSST-1 are shown in red. This figure was created using INSIGHT (Biosym Corp.).

wild type TSST-1 using rabbit splenocytes. Lower dosages produce reductions of up to 50% (*28*). In a previous paper (*29*), an 11−67% reduction in activity was reported. However, later resequencing showed that that mutant was the triple mutant T69I/Y80W/I140T. The T128A mutant was not found in the library of mutants reported by Hurley et al. (*32*). As shown in Table 2, the T128A mutant has proliferative activities on rabbit splenocytes which are uniformly less than that of the wild type and less than that of the I140T mutant at high concentrations. Both the T128A and I140T mutants show no reduction in lethality.

For the mutants in this class, the structural data presented here show no substantial conformational change. This suggests that lethality and superantigenicity can be jointly modulated simply by changing the character of the exposed surface near the top of domain A of TSST-1.

Papageorgiou et al. (*46*) suggested that the geometry of the Ser 15−Gly 16 peptide bond plays a key role in modulating superantigenicity. Our view is that these residues contribute to the TCR binding site of TSST-1 and thus can influence superantigenicity. However, it seems unlikely that the Ser 15−Gly 16 peptide geometry is the determining factor in superantigenicity. This bond is completely flipped in the Q136A mutant without the complete abolition of superantigenicity (see Table 2). Moreover, the addition of a side chain on residue 16 would stabilize the wild type (active) geometry since the ϵ main chain conformation (*50*) required by flipping the peptide bond would not be possible. This is not the case since the G16V mutant is not superantigenic (*32*).

Examination of the locations of mutations that control superantigenicity in TSST-1 suggests that there are differences in how TSST-1 and SEB bind class II MHC's and TCR's. Panels A and B of Figure 6 show the solvent accessible surfaces of TSST-1 and SEB, respectively. The Cα's in the barrel domain (B) have been used to obtain similar orientations. Residues shown to bind class II MHC (*16*, *17*) are on the front of the barrel domain. Since the structure of the SEB−TCR complex has not been published, we have used the structure of the SEC−TCR complex (*18*) to identify residues that bind the TCR since the SEB and SEC amino acid sequences are 66% identical. The corresponding TCR binding site for TSST-1 is indicated by those mutations outside the MHC-binding site that reduce superantigenicity (*28*−*30*, *32*, *49*). For SEB and TSST-1, the TCR binding site is on the top of the molecule behind a protruding ridge. For TSST-1, the ridge is formed by helix αA and so the presumed TCR site extends from the back of helix αA into a cleft formed with the β7−β9 loop and helix αB at the bottom. It is within this site where the T128A, H135A, Q139K, and I140T mutants discussed here are found. For SEB, the ridge is formed by the loop covering the front of the A domain and extends only to helix αA. As the sequence of the enterotoxins suggests that a large front loop is a common characteristic, we expect this difference in the geometry of the binding sites to be maintained.

Examples of mutants that modulate lethality and superantigenicity independently are Q136A (*28*, *29*) and the K132E mutant of TSST-ovine (T19A/A55T/T57S/T69I/Y80W/I140T TSST-1). Q136A retains about half of its superantigenicity despite showing no lethality. Conversely, the K132E mutant of TSST-ovine is as lethal as wild type TSST-1 while retaining only 10% of the wild type superantigenicity. This separability of lethality and superantigencity can be most easily explained by the presence of separate features controlling these properties. The observation that many mutants modulate superantigencity and lethality jointly suggests these features overlap. Since residue 136 is largely buried and does not change the electrostatic properties of the toxin, Occam's razor implies that the β7−β9 loop on the rear surface of TSST-1 forms part of the lethality-modulating feature. Verification of this hypothesis awaits the analysis of other mutants that demonstrate the independence of superantigenicity and lethality and the discovery of molecules that bind to this feature. This work is in progress.

ACKNOWLEDGMENT

We thank N. Elango and particularly Greg Vath for assistance in preparing the figures.

REFERENCES

1. Bergdoll, M. S., and Schlievert, P. M. (1984) *Lancet ii*, 691.
2. Cone, L. A., Woodard, D. R., Byrd, R. G., Schulz, K., Kopp, S. M., and Schlievert, P. M. (1992) *J. Infect. Dis. 165*, 638−643.
3. Newbould, M. J., Malam, J., McIllmurray, J. M., Morris, J. A., Telford, D. R., and Barson, A. J. (1989) *J. Clin. Pathol. 42*, 935−939.
4. Leung, D. Y. M., Meissner, H. C., Fulton, D. R., Murray, D. L., Kotzin, B. L., and Schlievert, P. M. (1993) *Lancet 342*, 1385−1388.
5. Burns, J. C., and Newburger, J. W. (1992) in *Infectious Diseases* (Gorbach, S. L., Bartlett, J. G., and Blacklow, N. R., Eds.) pp 1370−1374, W. B. Saunders Co., Philadelphia PA.
6. Bohach, G. A., Fast, D. J., Nelson, R. D., and Schlievert, P. M. (1990) *Crit. Rev. Microbiol. 17*, 251−272.
7. Schlievert, P. M., Bohach, G. A., Ohlendorf, D. H., Stauffacher, C. V., Leung, D. Y. M., Murray, D. L., Prasad, G. S., Earhart, C. A., Jablonski, L. M., Hoffmann, M. L., and Chi, Y.-I. (1995) *J. Clin. Immunol. 15*, 4S−10S.
8. Schad, E. M., Zaitseva, I., Zaitsev, V. N., Dohlsten, M., Kalland, T., Schlievert, P. M., Ohlendorf, D. H., and Svensson, L. A. (1995) *EMBO J. 14*, 3292−3301.
9. Swaminathan, S., Furey, W., Pletcher, J., and Sax, M. (1992) *Nature 359*, 801−806.
10. Swaminathan, S., Furey, W., Pletcher, J., and Sax, M. (1995) *Nat. Struct. Biol. 2*, 680−686.
11. Papageorgiou, A. C., Acharya, K. R., Shapiro, R., Passalacqua, R., Brehm, R. D., and Tranter, H. S. (1995) *Structure 3*, 769−779.
12. Bohach, G. A., Stauffacher, C. V., Ohlendorf, D. H., Chi, Y.-I., Vath, G. M., and Schlievert, P. M. (1996) *Adv. Exp. Med. Biol. 391*, 131−154.
13. Roussel, A., Anderson, B. F., Baker, H. M., Fraser, J. D., and Baker, E. N. (1997) *Nat. Struct. Biol. 4*, 635−643.
14. Prasad, G. S., Earhart, C. A., Murray, D. L., Novick, R. P., Schlievert, P. M., and Ohlendorf, D. H. (1993) *Biochemistry 32*, 13761−13766.
15. Acharya, K. R., Passalacqua, E. F., Jones, E. Y., Harlos, K., Stuart, D. I., Brehm, R. D., and Tranter, H. S. (1994) *Nature 367*, 94−97.
16. Jardetsky, T. S., Brown, J. H., Gorga, J. C., Stern, L. J., Urban, R. G., Chi, Y.-I., Stauffacher, C. V., Strominger, J. L., and Wiley, D. C. (1994) *Nature 368*, 711−718.
17. Kim, J., Urban, R. G., Strominger, J. L., and Wiley, D. C. (1994) *Science 266*, 1870−1874.
18. Fields, B. A., Malchiodi, E. L., Li, H., Ysern, X., Stauffacher, C. V., Schlievert, P. M., Karjalainen, K., and Mariuzza, R. A. (1996) *Nature 384*, 188−192.
19. Parsonnet, J., and Gillis, Z. A. (1988) *J. Infect. Dis. 158*, 1026−1033.
20. Poindexter, N. J., and Schlievert, P. M. (1985) *J. Infect. Dis. 151*, 65−72.
21. Fast, D. J., Schlievert, P. M., and Nelson, R. D. (1988) *J. Immunol. 140*, 949−953.
22. Schlievert, P. M., and Watson, D. W. (1978) *Infect. Immun. 21*, 753−763.
23. Fast, D. J., Schlievert, P. M., and Nelson, R. D. (1989) *Infect. Immun. 57*, 291−294.
24. Lee, P. K., Vercellotti, G. M., Deringer, J. R., and Schlievert, P. M. (1991) *J. Infect. Dis. 164*, 711−719.
25. Kim, Y. B., and Watson, D. W. (1970) *J. Exp. Med. 131*, 611−628.
26. Schlievert, P. M., Bettin, K. M., and Watson, D. W. (1980) *Infect. Immun. 27*, 542−548.
27. Schlievert, P. M. (1983) *J. Infect. Dis. 147*, 391−398.

28. Murray, D. L., Earhart, C. A., Mitchell, D. T., Ohlendorf, D. H., Novick, R. P., and Schlievert, P. M. (1996) *Infect. Immun. 64*, 371−374.
29. Murray, D. L., Prasad, G. S., Earhart, C. A., Leonard, B. A. B., Kreiswirth, B. N., Novick, R. P., Ohlendorf, D. H., and Schlievert, P. M. (1994) *J. Immunol. 152*, 87−95.
30. Blanco, L., Choi, E. M., Connolly, K., Thompson, M. R., and Bonventre, P. F. (1990) *Infect. Immun. 58*, 3020−3028.
31. Bonventre, P. F., Heeg, H., Cullen, C., and Lian, C.-J. (1993) *Infect. Immun. 61*, 793−799.
32. Hurley, J. M., Shimonkevitz, R., Hanagan, A., Enney, K., Boen, E., Kotzin, B. L., and Matsumura, M. (1995) *J. Exp. Med. 181*, 2229−2235.
33. Prasad, G. S., Radhakrishnan, R., Mitchell, D. T., Earhart, C. A., Dinges, M. M., Cook, W. J., Schlievert, P. M., and Ohlendorf, D. H. (1997) *Protein Sci. 6*, 1220−1227.
34. Blomster-Hautamaa, D. A., and Schlievert, P. M. (1988) *Methods Enzymol. 165*, 37−43.
35. Wlodawer, A., and Hodgson, K. O. (1975) *Proc. Natl. Acad. Sci. U.S.A. 72*, 398−399.
36. McPherson, A. (1982) *The Preparation and Analysis of Protein Crystals*, John Wiley, New York.
37. Earhart, C. A., Prasad, G. S., Murray, D. L., Novick, R. P., Schlievert, P. M., and Ohlendorf, D. H. (1993) *Proteins 17*, 329−334.
38. Howard, A. J., Gilliland, G. L., Finzel, B. C., Poulos, T. L., Ohlendorf, D. H., and Salemme, F. R. (1987) *J. Appl. Crystallogr. 20*, 383−387.
39. Brünger, A. T., Kuriyan, J., and Karplus, M. (1987) *Science 235*, 458−460.
40. Jones, T. A. (1978) *J. Appl. Crystallogr. 11*, 268−272.
41. Jones, T. A., Zou, J. Y., Cowan, S. W., and Kjeldgaard, M. (1991) *Acta Crystallogr. A47*, 110−119.
42. Mitchell, D. T., Schlievert, P. M., Ohlendorf, D. H., Kim, J., Wiley, D. C., Urban, R. G., and Strominger, J. L. (1996) in *Superantigens: Structure, Biology and Relevance to Human Disease* (Leung, D. Y. M., Huber, B. T., and Schlievert, P. M., Eds.) pp 149−166, Marcel Dekker, New York.
43. Chothia, C., and Lesk, A. M. (1986) *EMBO J. 5*, 823−826.
44. Ohlendorf, D. H. (1994) *Acta Crystallogr. D50*, 808−812.
45. Zhang, X. J., Wozniak, J. A., and Matthews, B. W. (1995) *J. Mol. Biol. 250*, 527−552.
46. Papageorgiou, A. C., Brehm, R. D., Leonidas, D. D., Tranter, H. S., and Acharya, K. R. (1996) *J. Mol. Biol. 260*, 553−569.
47. Brünger, A. T. (1992) *Acta Crystallogr. D49*, 24−46.
48. Bonventre, P. F., Heeg, H., Edwards, C. K., III, and Cullen, C. M. (1995) *Infect. Immun. 63*, 509−515.
49. Deresiewicz, R. L., Woo, J. H., Chan, M., Finberg, R. W., and Kasper, D. L. (1994) *Biochemistry 33*, 12844−12851.
50. Efimov, A. V. (1986) *Mol. Biol. (Moscow) 20*, 2250−2260.
51. Kraulis, P. J. (1991) *J. Appl. Crystallogr. 24*, 946−950.
52. Evans, S. V. (1993) *J. Mol. Graphics 11*, 134−138.

BI9721896